CHINESE OPTICS LETTERS

Vol. 21, No. 9 | September 2023

# Spectral manipulation in a high-power ultrafast fiber laser system generating ultrashort pulses with GHz repetition rate

Yingtao Zhang (张英韬)[1,†], Zihao Li (李子豪)[1,†], Tianxi Wang (王天玺)[1], Hao Xiu (修 昊)[1], Chiyi Wei (韦池一)[1], Luyi Wang (王麓屹)[1], Molei Hao (郝默雷)[1], Xiaoming Wei (韦小明)[1*], and Zhongmin Yang (杨中民)[1,2**]

[1] School of Physics and Optoelectronics, State Key Laboratory of Luminescent Materials and Devices, Guangdong Engineering Technology Research and Development Center of Special Optical Fiber Materials and Devices, Guangdong Provincial Key Laboratory of Fiber Laser Materials and Applied Techniques, South China University of Technology, Guangzhou 510640, China

[2] Research Institute of Future Technology, South China Normal University, Guangzhou 510006, China

*Corresponding author: xmwei@scut.edu.cn

**Corresponding author: yangzm@scut.edu.cn

Received April 24, 2023 | Accepted May 31, 2023 | Posted Online August 21, 2023

In this work, we demonstrate the spectral manipulation in an ultrafast fiber laser system that generates ultrashort pulses with a repetition rate of 1.2 GHz and two switchable modes—a 1064-nm fundamental laser mode with a maximum output power of 66.6 W, and a 1125-nm Raman laser mode with a maximum output power of 17.23 W. The pulse width, beam quality, and power stability are carefully characterized. We also investigate a method to switch between the two modes by manipulating the duty cycle of the modulation signal. It is anticipated that this bi-mode ultrafast fiber laser system can be a promising ultrafast laser source for frontier applications, such as micromachining, bioimaging, and spectroscopy.

**Keywords:** high power; high repetition rate; ultrafast fiber laser.
**DOI:** 10.3788/COL202321.091401

## 1. Introduction

High-power ultrafast fiber lasers have been used in many applications in a variety of fields, such as material processing, bioimaging, supercontinuum generation, and astronomical spectroscopy[1–10]. Compared with solid-state ultrafast lasers with free-space optics, ultrafast fiber lasers have advanced in cost efficiency, robustness, and maintenance, and thus they are highly desired for industrial applications, particularly in the field of material micromachining[11,12]. Recent studies have shown that the throughput and quality of the material micromachining can be significantly increased using the novel concept of ablation-cooling enabled by gigahertz (GHz)-repetition-rate ultrafast fiber laser at 1.0 μm[13]. In such a scenario, the successive high-repetition-rate ultrashort pulses arrive before the targeted spot cools down, such that they can efficiently ablate the hot spot. Similar demand for GHz-repetition-rate ultrashort pulses exists in the fields of biophotonics[14] and optical frequency comb spectroscopy[15]. In terms of the spectral window, the wavelength of 1.1 μm has drawn great interest, e.g., it was reported that fluorescence microscopy using 1.1-μm lasers had incomparable advantages in the fields of biomedical imaging[16,17] and micromachining in transparent materials[18].

There exist mainly two approaches to generate ultrafast fiber laser at 1.1 μm: supercontinuum generation using highly nonlinear fibers[19–23], or wavelength shifting inside or outside the laser cavities through nonlinear effects such as stimulated Raman scattering (SRS)[24–27]. The former approach manifests low power spectral density, and only a limited portion of the supercontinuum wavelength range is useful. Compared with supercontinuum generation, especially those using free-space configurations, the latter approach can enable high power efficiency, particularly without loss of compactness, which, however, has rarely been studied for generating high-power GHz-repetition-rate ultrashort pulses at 1.1 μm. To this end, here we present a bi-mode high-power GHz-repetition-rate ultrafast fiber laser source with a maximum output power of 66.6 W at 1.0 μm and 17.23 W at 1.1 μm. This fiber laser source can be flexibly switched between two output modes by adjusting the duty cycle of the modulation.

## 2. Experimental Setup

The schematic diagram of the bi-mode high-power ultrafast fiber laser system is presented in Fig. 1, which mainly includes:

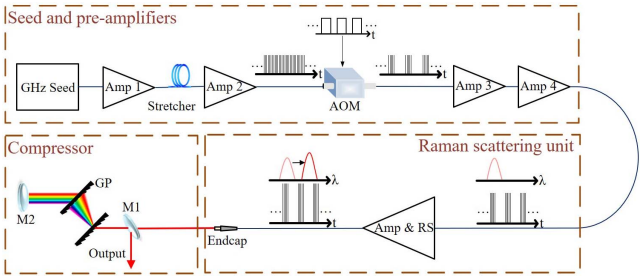


**Fig. 1.** Schematic setup of the high-power bi-mode femtosecond fiber laser. Amp, amplifier; AOM, acousto-optic modulator; RS, Raman scattering; M, mirror; GP, grating pair.

1) a GHz seed and four stages of pre-amplifiers, 2) a Raman scattering unit, and 3) a pulse compressor. The seed is passively mode locked and generates ultrashort pulses at 1064 nm. The seed oscillator cavity has a fiber length (~7.5 cm), corresponding to a fundamental repetition rate of 1.2 GHz, and it is pumped by a single-mode laser diode (II-IV, 974 nm wavelength, 680 mW maximum power). The seed oscillator cavity is housed in an environment with low humidity, low vibration, and suitable temperature to ensure long-term stability.

The seed has an average output power of ~1.0 mW, and it is subsequently connected to the four stages of pre-amplifiers. The first and second pre-amplifiers are configured with single-cladding gain fiber (Coractive Yb 401), while the third and fourth pre-amplifiers utilize double-cladding gain fiber (iXblue IXF-2CF-Yb-PM-6-130-NH and Nufern PLMA-YDF-10/125, respectively). After the first preamplifier, the average power of the signal can be boosted to ~60 mW. A long single-mode fiber (SMF, Corning HI1060, 200 m length) serving as a pulse stretcher, is placed between the first and second pre-amplifiers, which stretches the pulse width of the amplified GHz pulses to ~25 ps. After the stretcher, the average power decreases to ~20 mW, which is then boosted to ~100 mW by the second pre-amplifier. An acousto-optic modulator (AOM) driven by an arbitrary waveform generator (AWG), is placed after the second preamplifier to modulate the GHz pulse train, i.e., changing the continuous pulse train to bursts. In this study, the burst repetition rate is fixed at 1 MHz. In order to compensate for the power loss introduced by the AOM, the third preamplifier is applied, after which the average power becomes ~300 mW. The fourth preamplifier, which employs a double-cladding gain fiber and is pumped by two multimode laser diodes (II–IV, 974 nm wavelength, 9 W maximum power), is further used to amplify the average power to ~5 W. Fiber-based isolators (ISOs) are used at the end of the seed and each preamplifier to protect the laser system from the backward reflected light, which mainly consists of the amplified spontaneous emission (ASE).

In the Raman scattering unit, a main optical fiber amplifier is used to further increase the average power and shift the center wavelength to 1.1 μm (i.e., 1125 nm in this case), such that the fiber laser can be switched between two modes, i.e., a 1064-nm fundamental laser mode and a 1125-nm Raman laser mode, respectively, by modulating the pulse train with different duty cycles. In the main optical fiber amplifier, a polarization-maintaining large-mode-area fiber (Nufern PLMA-YDF-15/130-VIII, 15 μm core diameter) is used, and it is pumped by three high-power laser diodes (BWT, 976 nm wavelength, 60 W maximum power). After the Raman scattering unit, the signal power of the fundamental laser at 1064 nm is amplified from 5 to 66.6 W, and it can generate an average power of 17.23 W for the Raman laser at 1125 nm. To maintain the stable high-power operation of the bi-mode fiber laser, the Raman scattering unit is placed on a water-cooling platform. At the end, the GHz pulses are compressed by a grating pair (GP, transmission version, 1600 lines/mm).

## 3. Result and Discussion

To quantify the basic performance of the bi-mode fiber laser, its optical spectra at different conditions are measured with an optical spectrum analyzer (YOKOGAWA AQ6370B). A 2-GHz InGaAs photodetector (EOT ET-3010) is used to convert the optical signal of the laser pulses to an electrical signal, and then the pulse train is recorded with a 2-GHz real-time oscilloscope (LeCory 7200 A). The pulse width is measured with an autocorrelator (APE pulseCheck USB 50). The basic performance of the bi-mode fiber laser system is demonstrated in Figs. 2 and 3. Figure 2(a) shows the optical spectrum of the seed, while Fig. 2(b) shows the optical spectrum over a wider spectral span. The wavelength of the seed laser is centered at 1064 nm with a 3-dB bandwidth of 2.37 nm, corresponding to a transform-limited pulse width of ~501 fs, assuming a $\mathrm{sech}^2$-pulse shape. As shown in Fig. 2(c), the duration of each burst cycle is 1 μs, in accordance with the burst repetition rate of 1 MHz. The inset of Fig. 2(c) shows the pulse train over a time span of 10 ns in a burst envelope. The pulse width at 66.6 W in 1064-nm mode before

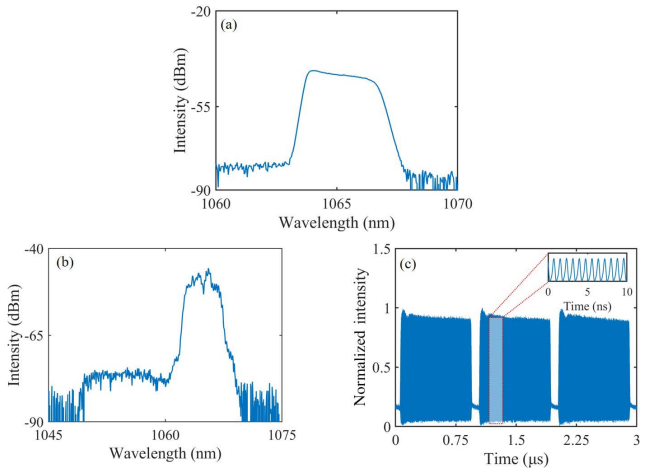


**Fig. 2.** (a) Optical spectrum of the seed, measured at the output of the seed. (b) The optical spectrum when laser power is 66.6 W, measured after the end cap. The spectral resolution of both (a) and (b) is 0.02 nm. (c) The pulse train of the laser source operating at the burst mode with a duty cycle of 90%. The inset shows the intrapulses in the burst envelope.

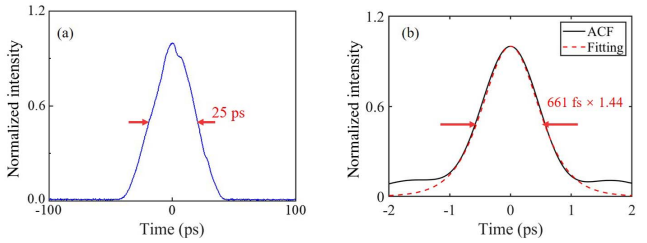


**Fig. 3.** (a) Pulse profile at the 1064-nm band before compression, measured at an output power of 66.6 W. (b) ACF measured at an output power of 40.82 W and a duty cycle of 90%.

compressing is presented in Fig. 3(a), and the full width at half-maximum is measured to be ~25 ps. The autocorrelation function (ACF) of the ultrashort pulses after compression is shown in Fig. 3(b). The full width at half-maximum of the compressed pulses is measured to be 661 fs, assuming a sech$^2$-pulse shape. When modulating with a duty cycle of 90%, the nonlinear effect is not significant at a relatively low peak power, and thus the optical spectrum is centered at 1064 nm without obvious wavelength shifting produced by the nonlinear effect, as shown in the inset of Fig. 2(a).

The power stability at the maximum output power and the slope efficiency curve of the bi-mode ultrafast fiber laser source operating in the 1064-nm fundamental laser mode are shown in Figs. 4(a) and 4(b), respectively, measured by a fan-cooled thermal power meter (Ophir FL1100A-BB-65). The standard deviation of the output power is quantified to be less than 0.29% over a time span of 8 h at the maximum output power of 66.6 W (before compressing). As shown in Fig. 4(b), the main optical fiber amplifier can deliver an output power up to 66.6 W at a pump power of 91.8 W, and the corresponding slope efficiency is calculated to be 77.38%. The beam quality $M^2$ measured with a CCD camera mounted on a linear translation stage is shown in Fig. 4(c). The beam quality $M^2$ of the output

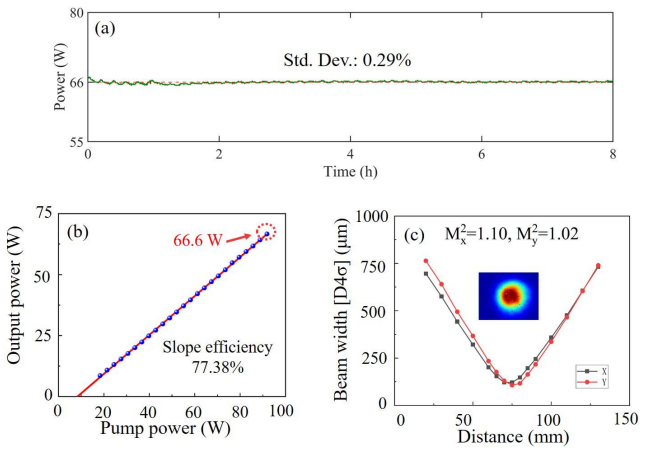


**Fig. 4.** Performance of the fundamental wavelength component (i.e., 1064 nm). (a) Long-term power stability of the main optical fiber amplifier measured at an output power of 66.6 W (before compressing). (b) Slope efficiency. (c) Laser beam quality $M^2$ measurement.

laser beam is calculated to be 1.10 and 1.02 for the $x$ and $y$ directions, respectively.

By changing the duty cycle of the burst modulation to a lower value, a stronger nonlinear effect can be obtained, resulting from the relatively high peak power of the ultrashort pulses, such that the optical wavelength of the fiber laser source can be efficiently shifted to 1125 nm. It should be pointed out that the fiber laser source also benefits from the modulation of the AOM and the relatively small core diameter of the gain fiber in the Raman scattering unit. Moreover, the operation mode of the fiber laser source can be easily switched by adjusting the duty cycle of the burst modulation. The spectral evolution of the ultrafast fiber laser source with the pump power increasing or duty cycle changing is shown in Figs. 5(a) and 5(b). From top to bottom, the average output powers of the fiber laser source at the 1.1-μm wavelength window are 0.018, 1.926, 11.56, and 17.23 W, respectively. In this measurement, the duty cycle of the burst modulation is fixed at 10%. Before turning on the main optical fiber amplifier, the wavelength component at 1125 nm is relatively weak. By increasing the pump power of the main optical fiber amplifier, the wavelength component at 1125 nm starts to grow and broaden because of the enhanced SRS effect. When the output power reaches its maximum, the 3-dB bandwidth at the center wavelength of 1125 nm is about 9.91 nm, corresponding to an ideal transform-limited pulse width of ~132 fs. After spectral filtering, the fundamental wavelength component (i.e., centered at 1064 nm) is more than 10 dB lower than that of the SRS-shifted wavelength component (i.e., centered at 1125 nm). Please note that a higher suppression ratio can be achieved by cascading more spectral filters or using a spectral filter with better optical density. Figure 5(b) shows the spectral evolution of the ultrafast fiber laser source when duty cycles are 90%, 50%, 20%, and 10%, respectively. As can be observed, the optical spectrum does not exhibit notable change when the duty cycle is within the range between 90% and 50%. SRS emerges only when the duty cycle is tuned below 50%, and significant changes in the optical spectrum can be observed only when the duty cycle is tuned below 20%.

The performances of the 1125-nm wavelength component of the bi-mode ultrafast fiber laser source are also measured and demonstrated in Fig. 6. The relationship between the output power of the 1125-nm wavelength component and the power of the 1064-nm fundamental wavelength component is depicted in Fig. 6(a). The slope efficiency is calculated to be 61.35%, and a maximum output power of 17.23 W can be achieved for a driving power of 40.82 W at the fundamental wavelength component at 1064 nm, corresponding to an optical–optical conversion efficiency of ~42%. It should be pointed out that, considering the potential damage of the optical items at 1125 nm, the optical power of the fundamental 1064-nm beam is not increased to the maximum value (i.e., 66.6 W). Figure 6(b) depicts the beam quality $M^2$ measurement, i.e., 1.33 and 1.17 for $x$ and $y$ directions, respectively. The inset shows beam profile of the 1125-nm wavelength component after spectral filter, which exhibits an ellipticity of 0.957.

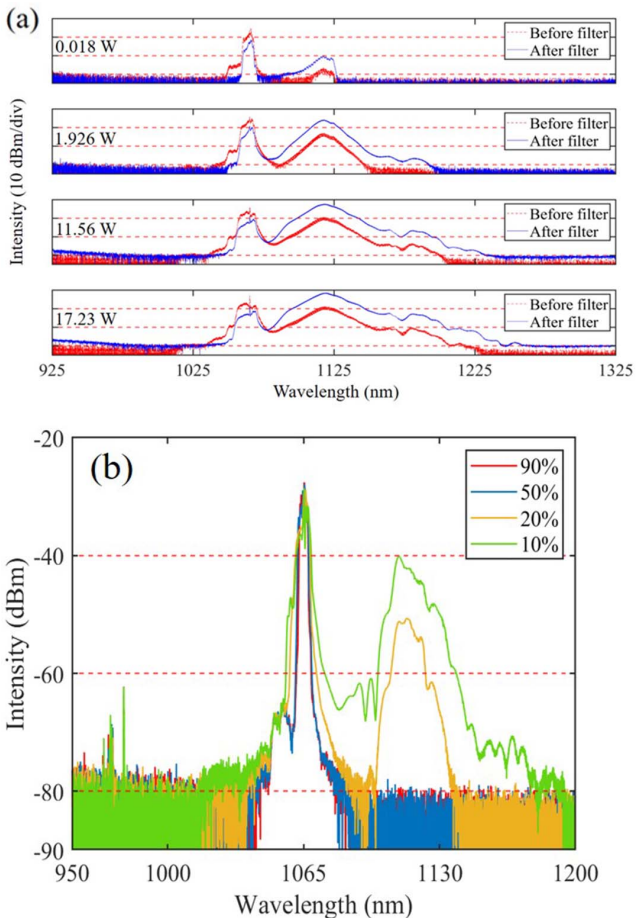


**Fig. 5.** (a) Optical spectra of the fiber laser source operating with a duty cycle of 10%; from top to bottom, the average output powers at ~1.1 μm are 0.018, 1.926, 11.56, and 17.23 W, respectively. (b) Optical spectra with duty cycles of 90%, 50%, 20%, and 10%, respectively.

## 4. Conclusion

In this Letter, we have reported a bi-mode femtosecond fiber laser source with a repetition rate of 1.2 GHz, which has a maximum output power of 66.6 W at the 1064-nm fundamental laser mode and a maximum power of 17.23 W at the 1125-nm Raman laser mode. The operation of the fiber laser source can be manipulated by the burst modulation, and the 1125-nm Raman laser can be efficiently generated by leveraging the SRS effect. With promising performance, including good beam quality and long-term power stability, this high-power and high-repetition-rate femtosecond laser source in all-fiber configuration is expected to be a good alternative to industrial applications.

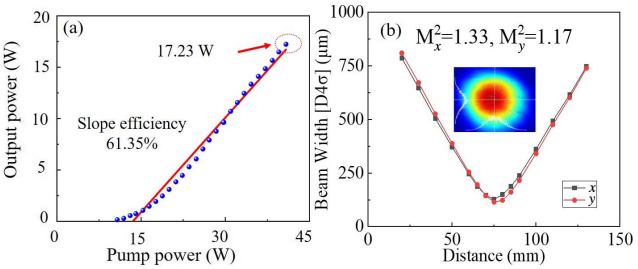


**Fig. 6.** Performances of the 1125-nm wavelength component. (a) Slope efficiency; (b) beam quality $M^2$ measured at an output power of 17.23 W and a duty cycle of 10%. The inset shows the laser beam profile.

## Acknowledgement

This work was supported by the NSFC Development of National Major Scientific Research Instrument (No. 61927816), the Introduced Innovative Team Project of Guangdong Pearl River Talents Program (No. 2021ZT09Z109), the Natural Science Foundation of Guangdong Province (No. 2021B1515020074), the Mobility Programme of the Sino-German (No. M-0296), the Double First Class Initiative (No. D6211170), the National Natural Science Foundation of China (Nos. U1609219 and 62235014), the Science and Technology Project of Guangdong (No. 2020B1212060002), and the Key R&D Program of Guangzhou (No. 202007020003).

†These authors contributed equally to this work.

## References

1. D. Strickland and G. Mourou, "Compression of amplified chirped optical pulses," Opt. Commun. **55**, 447 (1985).
2. G. R. Kumar, "The 2018 Nobel prize in physics: a gripping and extremely exciting tale of light," Curr. Sci. **115**, 1844 (2018).
3. G. Bonamis, G. Bonamis, E. Audouard, C. Hönninger, J. Lopez, K. Mishchik, E. Mottay, and I. Manek-Hönninger, "Systematic study of laser ablation with GHz bursts of femtosecond pulses," Opt. Express **28**, 27702 (2020).
4. G. A. Mourou, T. Tajima, and S. V. Bulanov, "Optics in the relativistic regime," Rev. Mod. Phys. **78**, 309 (2006).
5. D. F. Farson, H. W. Choi, B. Zimmerman, J. K. Steach, J. J. Chalmers, S. V. Olesik, and L. J. Lee, "Femtosecond laser micromachining of dielectric materials for biomedical applications," J. Micromech. Microeng. **18**, 035020 (2008).
6. S. H. Chung and E. Mazur, "Surgical applications of femtosecond lasers," J. Biophoton. **2**, 557 (2009).
7. T. Harada, S. Spence, A. Margiolakis, S. Deckoff-Jones, R. Ploeger, A. Shugar, J. Hamm, K. Dani, and A. Dani, "Obtaining cross-sections of paint layers in cultural artifacts using femtosecond pulsed lasers," Materials **10**, 107 (2017).
8. A. Dubietis, A. Couairon, and G. Genty, "Supercontinuum generation: introduction," J. Opt. Soc. Am. B **36**, SG1 (2019).
9. T. Steinmetz, T. Wilken, C. Araujo-Hauck, R. Holzwarth, T. W. Hänsch, L. Pasquini, A. Manescau, S. D'Odorico, M. T. Murphy, T. Kentischer, W. Schmidt, and T. Udem, "Laser frequency combs for astronomical observations," Science **321**, 1335 (2008).
10. Q. Gong and W. Zhao, "Ultrafast science to capture ultrafast motions," Ultrafast Sci. **2021**, 9765859 (2021).
11. K. C. Phillips, H. H. Gandhi, E. Mazur, and S. K. Sundaram, "Ultrafast laser processing of materials: a review," Adv. Opt. Photon. **7**, 684 (2015).
12. Z. Lin and M. Hong, "Femtosecond laser precision engineering: from micron, submicron, to nanoscale," Ultrafast Sci. **2021**, 9783514 (2021).
13. C. Kerse, H. Kalaycıoğlu, P. Elahi, B. Çetin, D. K. Kesim, Ö. Akçaalan, S. Yavaş, M. D. Aşık, B. Öktem, H. Hoogland, R. Holzwarth, and F. Ö. Ilday, "Ablation-cooled material removal with ultrafast bursts of pulses," Nature **537**, 84 (2016).
14. N. Ji, J. C. Magee, and E. Betzig, "High-speed, low-photodamage nonlinear imaging using passive pulse splitters," Nat. Methods **5**, 197 (2008).

15. T. Fortier and E. Baumann, "20 years of developments in optical frequency comb technology and applications," Commun. Phys. **2**, 153 (2019).
16. Y. Tang, F. Pei, X. Lu, Q. Fan, and W. Huang, "Recent advances on activatable NIR-II fluorescence probes for biomedical imaging," Adv. Opt. Mater. **7**, 1900917 (2019).
17. K. Gao, Y. Liu, W. Qiao, R. Xu, T. Feng, H. Xuan, D. Li, X. Zhao, A. Wang, and T. Li, "Sub-60-fs, compact 1100-nm fiber laser system based on double-pass pre-chirp managed amplification," Opt. Lett. **47**, 5016 (2022).
18. S. M. Kobtsev, S. V. Kukarin, Y. S. Fedotov, and A. V. Ivanenko, "High-energy femtosecond 1086/543-nm fiber system for nano- and micromachining in transparent materials and on solid surfaces," Laser Phys. **21**, 308 (2011).
19. Y. Yang, W. Bi, X. Li, M. Liao, W. Gao, Y. Ohishi, Y. Fang, and Y. Li, "Ultrabroadband supercontinuum generation through filamentation in a lead fluoride crystal," J. Opt. Soc. Am. B **36**, A1 (2019).
20. R. Šuminas, A. Marcinkevičiūtė, G. Tamošauskas, and A. Dubietis, "Even and odd harmonics-enhanced supercontinuum generation in zinc-blende semiconductors," J. Opt. Soc. Am. B **36**, A22 (2019).
21. V. Jukna, N. Garejev, G. Tamošauskas, and A. Dubietis, "Role of external focusing geometry in supercontinuum generation in bulk solid-state media," J. Opt. Soc. Am. B **36**, A54 (2019).
22. G. Soboń, R. Lindberg, V. Pasiskevicius, T. Martynkien, and J. Sotor, "Shot-to-shot performance analysis of an all-fiber supercontinuum source pumped at 2000 nm," J. Opt. Soc. Am. B **36**, A15 (2019).
23. S. Zhang, M. Jiang, C. Li, R. Su, P. Zhou, and Z. Jiang, "High-power broadband supercontinuum generation through a simple narrow-bandwidth FBGs-based fiber laser cavity," Chin. Opt. Lett. **20**, 011405 (2022).
24. S. Kimura, S. Tani, and Y. Kobayashi, "Raman-assisted broadband mode-locked laser," Sci. Rep. **9**, 3738 (2019).
25. X. Yang, L. Zhang, H. Jiang, T. Fan, and Y. Feng, "Actively mode-locked Raman fiber laser," Opt. Express **23**, 19831 (2015).
26. A. G. Kuznetsov, D. S. Kharenko, E. V. Podivilov, and S. A. Babin, "Fifty-ps Raman fiber laser with hybrid active-passive mode locking," Opt. Express **24**, 16280 (2016).
27. P. G. Zverev, T. T. Basiev, and A. M. Prokhorov, "Stimulated Raman scattering of laser radiation in Raman crystals," Opt. Mater. **11**, 335 (1999).